Volume 1 | Number 1 | Jan 2013 | Pages 1–100

Journal of
Materials Chemistry B

Materials for biology and medicine
www.rsc.org/materialsB

ROYAL SOCIETY
OF CHEMISTRY

ROYAL SOCIETY
OF CHEMISTRY

www.rsc.org/materialsB

Journal of Materials Chemistry B

Paper

Confinement controlled mineralization of calcium carbonate within collagen fibrils

Hang Ping,[a] Hao Xie,[b*], Yamin Wan,[a] Zhixiao Zhang,[a] Jing Zhang,[a] Mingyu Xiang,[a] Jingjing Xie,[a] Hao Wang,[a] Weimin Wang,[a] Zhengyi Fu[a*]

Confinement is common in biological systems and plays a critical role in the structure-forming process of biominerals. However, the knowledge of confinement effects on biomineralization is limited due to the lack of specific chemical structures and elaborate spatial distribution. In this article, we explore the confined mineralization of amorphous calcium carbonate (ACC) within collagen fibrils. Three issues of confined mineralization of ACC within collagen fibrils were investigated, including morphology and characteristics of confined mineralization of ACC within collagen fibrils; initiation and development of confined mineralization of ACC within collagen fibrils; and the driving mechanism of ACC infiltration into collagen fibrils. Results show that the negatively charged ACC droplets were attracted to positively charged gap regions of collagen fibrils through electrostatic interaction, infiltrated into collagen fibrils, and then transformed into crystalline phase. The observation of juxtaposed crystalline and amorphous phases on the surface of fibrils indicates that a secondary nucleation mechanism may be responsible for the co-orientation of calcite nanocrystals. Through modifying the wettability of amorphous calcium carbonate with magnesium ions, it is verified that the infiltration of ACC into collagen fibrils was driven by capillary forces. The present study not only provides evidence of the confinement effects in biomineralization but also facilitates the understanding of the *in vivo* bone formation process. It may also open a new avenue in bioprocess-inspired synthesis of advanced materials.

Introduction

Biominerals, such as bone, teeth, and shells, exhibit exquisite hierarchical structures and outstanding mechanical properties.[1] Attracted by the unique structures of biominerals, scientists have successfully designed and fabricated "bio-inspired materials".[2-4] Furthermore, the fantastic structure-forming process in biological systems is the evolution results of many billions of years, which efficiently and accurately fabricate biominerals under environmentally benign conditions. Taking lessons from the natural structure-forming process of biominerals, one can find ideas for developing bioprocess-inspired synthesis techniques for advanced materials.[5-9]

Biomineralization is a temporally and spatially regulated process that involves functions of living organisms and forming of minerals.[10] Organic matrix usually acts as the framework or template to allow the deposition and mineralization of inorganic substances under the function of soluble proteins.[11] For example, the formation of a mollusk shell is based on highly ordered chitin matrix with associated silk protein and acidic glycoproteins that direct crystal morphology, orientation, and

polymorph type.[12] It was also observed that amorphous calcium carbonate plays important roles in creating the unique structure during the forming process of spine.[13] Jong Seto et al. reported that a sea urchin's spine with non-equilibrium morphology diffracts as a single crystal and shows a glassy fracture surface, which challenges the classical expectation of a single crystal behavior.[14] In addition to the observation of amorphous phases during the structure-forming process of biominerals, it is noted that confinement at different levels is one of the important features of biomineralization, such as calcium oxalate growth in human kidneys,[15] silica formation in diatoms,[16] and apatite ordered organization within collagen fibrils.[5] Localization of biominerals and their functions are greatly determined and affected by confinement. It is essential to investigate the process and mechanisms of confinement provided by biological environments in biomineralization in order to better understand biomineral-forming in living organisms.[17]

Scientists studied the process and mechanisms of confined biomineralization and made important observation.[17-21] Maas *et al.* have developed a one-step process for preparing mineralized nanofibers of collagen fibrils containing calcium phosphate.[17] The nanofibers resemble closely the same structure found in bone, which might be promising for future tissue engineering study and new structure designing of composite materials. Meldrum *et al.* obtained highly aligned nanowires from amorphous calcium carbonate or amorphous calcium phosphate precipitation by porous membranes as templates.[18,20,21] The designing and results are helpful in

a. State Key Laboratory of Advanced Technology for Materials Synthesis and Processing, Wuhan University of Technology, Wuhan, 430070, China. *E-mail address: zyfu@whut.edu.cn.
b. School of Chemistry, Chemical Engineering, and Life Science, Wuhan University of Technology, Wuhan, 430070, China. *E-mail address: h.xie@whut.edu.cn.

ARTICLE

understanding the driving force of amorphous phase penetrating into pores, the aspect ratio of nanowires, and the polymorph of products.

Comparing with simple and effective artificial systems for elucidating the confinement, biological systems are more complicated due to specific chemical structures and elaborate spatial distribution.[22] Studying confinement effects in a biological organism can lead to find natural interesting phenomena which may not occur in an artificial system. A suitable model systems is critical in elucidating the mechanism of confined biomineralization.

Intrafibrillar mineralization of apatite can be considered as a confined biomineralization process. Mineralized collagen fibrils are the basic building blocks of bone, which are hierarchically arranged from the nanometer to the macroscopic length scales.[23] The mineralized fibrils contain nanosize apatite crystals and fibrous collagen fibril, and the nanocrystals embed within organic matrix and orient along its longitude axis. The interaction between apatite and collagen fibril at multi-scale level provides bone with strength and toughness.[24] It is known that acidic non-collagen proteins (NCPs) play important roles during the process of bone formation.[25] The high content of acidic amino acid of NCPs facilitate the formation and stabilization of amorphous precursors, then the amorphous precursors infiltrate into collagen fibrils and transform into apatite crystals. The precise quarter-staggered array of tropocollagen molecular endows a 40 nm long gap region of collagen fibrils with positive charges that promote the infiltration of negatively charged amorphous precursors.[26,27] Inspired by the role of collagen fibrils in bone formation, intrafibrillar mineralization of various minerals has been achieved, including silica,[28] yttria-stabilized zirconia[29] and silica-apatite multiphase.[30] However, this process remains elusive for both collagen fibrils mineralization and the driving force of the infiltration of amorphous precursor.

In the present study, we explored the confinement controlled mineralization of ACC within collagen fibrils on account of several factors: (1) the calcium carbonate mineralization is a popular biomineralization model system, and the transformation of ACC has been extensively investigated; (2) the polymorph of calcium carbonate can be clearly identified; and (3) the chemical composition of ACC can be comfortably modified by different additives to facilitate handling the crystallization process.[11] Three issues of confined mineralization of ACC within collagen fibrils were investigated, including: (1) morphology and characteristics of confined mineralization of ACC within collagen fibrils (i.e., intrafibrillar collagen mineralization of calcium carbonate); (2) initiation and development of confined mineralization of ACC within collagen fibrils (i.e., infiltration and transformation of ACC); and (3) the driving mechanism of ACC infiltration into collagen fibrils.

Experimental

Assembly of collagen fibrils

Collagen stock solution was prepared by dissolving lyophilized type I collagen powder (C9791, Sigma-Aldrich, USA) in 0.1 M acetic acid at 4 °C overnight. Then 30 µL aliquot of collagen stock solution was deposited on poly(lysine)-coated glass coverslips. The reconstitution was initiated by neutralizing the collagen stock solution with ammonia vapour in a humidity chamber for 3 h. Subsequently, the ammonium hydroxide solution was removed and the collagen solution was incubated at room temperature for 21 h.

Preparation of reaction solution

Mineralization of calcium carbonate inside collagen fibrils was in solutions containing polyacrylic acid (Alfa-Aesar, USA). Solution A containing 20 mM N-(2-Hydroxyethyl)piperazine-N'-(2-ethanesulfonic acid) (Hepes), 20 mM $CaCl_2$, (Sinopharm, China), and 200 µg mL^{-1} polyacrylic acid (Alfa-Aesar, USA) was titrated into equal volume solution B containing 20 mM Na_2CO_3, 300 mM NaCl at a rate of 6 s per drop. The pH was adjusted to 7.4 with 0.1 M NaOH. The final concentration of Ca^{2+} and CO_3^{2-} ions was 10 mM. The control group was solution A without polyacrylic acid. For testing the effects of Mg^{2+}, the ratio of Mg^{2+}/Ca^{2+} was 1/1 at constant 5 mM Ca^{2+} in solution A.

Mineralization of collagen fibrils

Reconstituted collagen fibrils coated glass coverslips were incubated in mineralization solution at 37 °C for 1-3 days. The time-course of the reaction was investigated over a 1 day interval. The coverslips were washed three times with deionized water, and dried in air for further characterization.

Characterization of mineralized collagen fibrils

Mineralized collagen fibrils coated coverslips were fixed on aluminum stubs with carbon pads and sputter-coated with platinum for 30 seconds. Surface morphological information was provided by field emission scanning electron microscopy (FESEM) using a Hitachi S-4800 at 5 kV. Energy-dispersive spectroscopy (EDS) detector was coupled with a scanning electron microscope (SEM), and used to analyze the elemental composition of the mineralized samples. The phase composition and crystallinity of products were examined by X-ray diffraction (XRD) using Bruker D8 Advance, equipped with Cu Kα radiation (V = 40 kV, I = 40 mA). The diffraction patterns were collected in the range of 10-80 degree, with a scan step of 0.5 degree/minute. The formation of calcium carbonate polymorphs inside collagen fibrils was evaluated with Fourier Transform infrared spectroscopy (FTIR) on a ThermoScientific Nicolet 6700. Samples scratching from coverslips grinded with potassium bromide and pressed mixture into pellets. The FTIR spectra of pellets were collected from 4000 to 400 cm^{-1}, at a resolution of 4 cm^{-1} with 32 scans. The information of calcium carbonate polymorphs was also recorded by using a Renishaw InVia Raman spectrometer. The excitation source was an Nd:YAG laser operating at 785 nm and focused onto samples with a 50x objective. The samples were dispersed in alcohol through ultrasonic treatment and then transferred directly to

ultrathin carbon coated copper grids. The fine structure of isolated collagen fibril was investigated with high-resolution transmission electron microscopy (HRTEM) on a JEM 2100F at 200 kV. The phase identification of mineralization products was obtained by using selected area electron diffraction techniques (SAED). The size distribution and surface charge of amorphous calcium carbonate and magnesium ions added amorphous calcium carbonate in the reaction solution after 3 h were determined by dynamic light scattering (DLS) and Zeta potential by using a Malvern Zetasizer 3000HS.
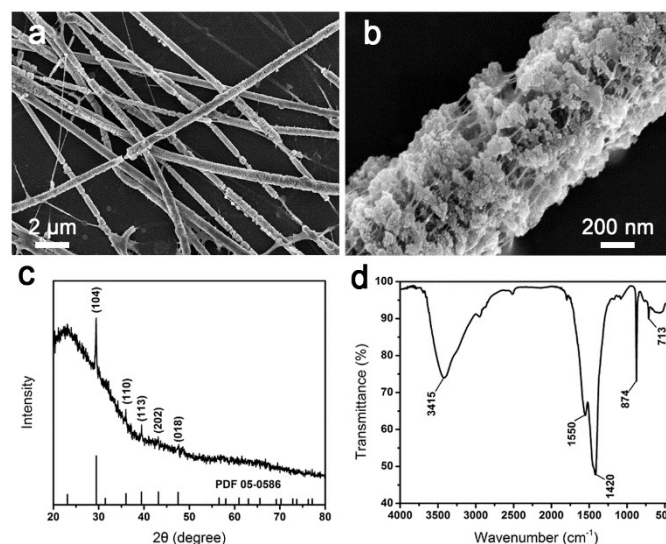

Fig. 1. Mineralization of reconstituted collagen fibrils. (a) Low and (b) high magnification SEM images of mineralized collagen fibrils. (c) XRD and (d) FTIR patterns of mineralized collagen fibrils.

Results and discussion

Intrafibrillar collagen mineralization of calcium carbonate

Intrafibrillar collagen mineralization of calcium carbonate was achieved by incubating reconstituted collagen fibrils in mineralization solution containing 100 µg mL^{-1} polyacrylic acid for 72 h (Fig. 1a). The high magnification SEM image shows that nanocrystals with dimension of 14.2±3.8 nm nm deposit on the surface of collagen fibrils (Fig. 1b). The diameter of fibril changed from 201.6±40.2 nm before mineralization (Fig. S1) to 793.0±156.8 nm after intrafibrillar mineralization. The swell of collagen fibrils during mineralization could be resulted from the penetration of nanocrystals into collagen fibrils. The liquid-crystalline nature of collagen allowed sufficient flexibility for the tropocollagen molecules to be pushed aside.[31] The pores were then exposed on the collagen surface. The existence of nanocrystals was obviously observed within the fibril from a cross sectional view of broken fibrils (Fig. S2). The crystalline phase of minerals formed in 72 h was indexed as calcite (JCPDS No. 05-0586) with the XRD pattern shown in Figure 1c. The FTIR spectrum showed two characteristic bands at 1420 cm^{-1} and 874 cm^{-1} that correspond to the $v3$ and $v2$ modes of calcium carbonate. Another two peaks at 1550 cm^{-1} and 713 cm^{-1} were assigned to the characteristic of amide I of collagen and crystalline calcite, respectively (Fig. 1d).[32]

The tip of the mineralized fibril is composed of densely packed nanocrystals (Fig. 2a). The magnified TEM image (Fig. 2b) shows that the size of nanocrystals is consistent with SEM data. The related SAED pattern exhibits characteristic diffraction spots of the rhombohedral structure of calcite (Fig. 2c inset). The crystal lattice with interplanar spacing of 0.30 nm corresponds to the (104) plane of calcite (Fig. 2c). Although the mineralized fibril contained nanoparticle units, it did not exhibit the typical ring pattern of polycrystalline calcite. This indicates that the nanoparticle building blocks were highly oriented and aligned. The slightly arc-shaped diffraction spots manifested that there was small lattice distortion between the boundaries of the nanoparticles.[33] The HRTEM image of nanoparticles shows some mosaic domains disturbing the continuity of the lattice planes (white arrows). These mosaic domains may be porous among nanoparticle units. The continuous lattice fringes in Figure 2c also demonstrate the high orientation of nanoparticles.

This journal is © The Royal Society of Chemistry 2015

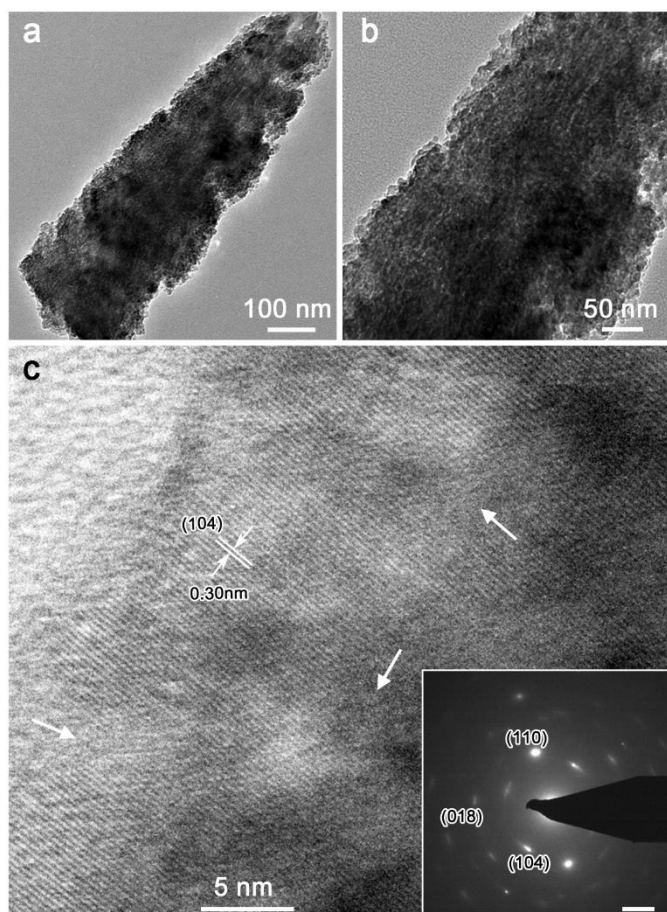*J. Mater. Chem. B*, 2015, **00**, 1-3 | **3**

Fig. 2. TEM images of individual mineralized fibril. (a) Low and (b) high magnification TEM images of the tip of mineralized fibrils. (c) HRTEM image and SAED pattern of mineralized fibril.

We further investigated the time course of infiltration of nanocrystals into collagen fibrils. Deposition of minerals was observed as spherical droplets of different sizes in 24 h of mineralization (Fig. S3a). Tiny droplets tended to aggregate and coalesce into large ones. The surface of collagen fibrils was covered with droplets (Fig. 3a) that wet the collagen fibrils as well.[34] Due to the effects of the coating of a large amount of amorphous phase on fibril surface, no obvious peaks of crystalline phase were observed in 24 h (Fig. S4). After 48 h of mineralization, spherical droplets still existed around collagen fibrils (Fig. S3b). However, gradual infiltration of droplets into fibril was observed, as well as the appearance of nanocrystals on the surface and inside the fibrils (Fig. 3b). A weak and broad peak at 29 degree was visible in 48 hours (Fig. S4).

In the present study, the formation of spherical droplets was through the polymer induce liquid precursor (PILP) process, and a large number of droplets aggregate together (Fig. S5a). Closely contacted droplets could form larger ones (Fig. S5b). The smooth surface of droplets and the connecting neck between these droplets manifested the coalescing of these droplets.[35] TEM image shows that small droplets aggregate in the vicinity of large droplets (Fig. S5c), suggesting a liquid-like behavior of these droplets.[36] The amorphous nature of these droplets was revealed with selected area electron diffraction (Fig. S5d). Energy dispersive spectroscopy (Fig. S5e) indicated the chemical elements of these droplets were calcium, oxygen and carbon. Based on these results, these spherical droplets were inferred as amorphous calcium carbonate. The calcite was not formed in 24 h of mineralization since no characteristic peak of FTIR spectrum was observed at 713 cm^{-1} (Fig. 3c). However, there was a peak at 1080 cm^{-1}, implying the presence of amorphous phase.[32] Within 48 h of mineralization, the two peaks at 713 cm^{-1} and 1080 cm^{-1} were observed in the FTIR spectrum, indicating the presence of both calcite and amorphous phase are in collagen fibrils (Fig. 3d). This result demonstrates that a phase transformation occurred from amorphous phase into calcite.
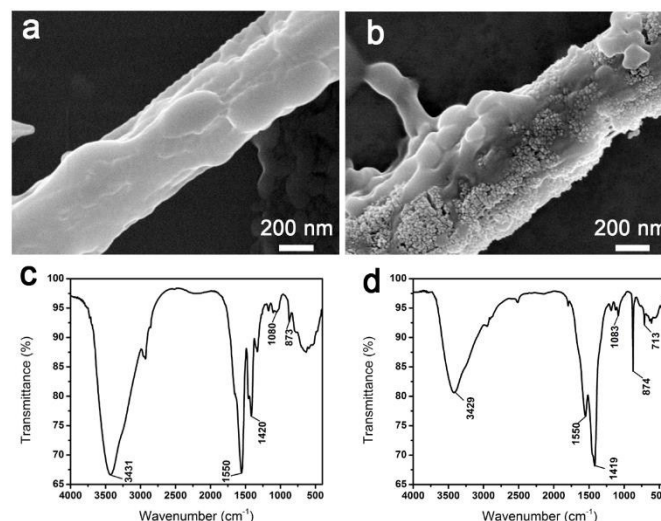

Fig. 3. Mineralization of reconstituted collagen fibrils. (a) Low and (b) high magnification SEM images of collagen fibrils after 24 h of mineralization. (c) Low and (d) high magnification SEM images of collagen fibrils after 48 h of mineralization. FTIR patterns of collagen fibrils after (e) 24 h and (f) 48 h of mineralizaiton.

The importance of polyacrylic acid in confined mineralization of calcium carbonate within collagens was also demonstrated. If polyacrylic acid was not included in the mineralization system, it would result the deposition of bulk crystals with rhombohedral morphology (Fig. S6a). XRD patterns show that rhombohedral crystalline phase is calcite. The preferred orientation of calcite crystals was indicated by the intensive peak of the (104) plane (Fig. S7). A higher magnification image of the step surface of calcite shows that the crystals consisted of an agglomeration of nanoparticles (Fig. S6b). This surface texture hints that the continuous growth of the calcite crystals occurs through primary particle accretion.[37] Meanwhile, collagen fibrils intertwined on the surface of calcite. The characteristic band pattern of collagen is distinct, and the fibrils are shrivelled.

In a mineralization system containing aspartic acid instead of poly(acrylic acid), the truncated calcite crystals deposit on the coverslip (Fig. S8 and S9). No intrafibrillar mineralization has been observed. This is due to that the monomer can not direct the polymer-induced liquid precursor process. When replacing poly(acrylic acid) with another negatively charged polymers, such as ovalbumin or poly(styrene sulfonate) in the mineralization system, resultant morphology and polymorph of calcium carbonate are different to that of poly(acrylic acid).

4 | *J. Mater. Chem. B*, 2015, **00**, 1-3

This journal is © The Royal Society of Chemistry 2015

Please do not adjust margins

There is still no intrafibrillar mineralization of calcium carbonate has been achieved (Fig. S10 and S11). Properties of additives including molecular weight, concentration, and charge distribution may affect the mineralization. Comparing with other negatively charged polymers, the functional group of poly(acrylic acid) is carboxyl and is more efficient in interacting with Ca^{2+}. Above results suggest that poly(acrylic acid) is essential for growth of calcium carbonate inside collagen fibrils. The confined mineralization was also investigated at reduced concentrations of inorganic ions (that is, 5 mM or 2 mM of Ca^{2+} and CO_3^{2-}). When no poly(acrylic acid) was included in the mineralization system, deposition of the rhombohedral calcite crystal was observed on the surface of coverslips (Fig. S12 and S13). The bend and shrivelled fibrils indicate that the intrafibrillar mineralization of calcium carbonate does not occur. When including poly(acrylic acid) in the mineralization system, the mineral crystals disappeared and the collagen fibrils adhered to the coverslip (Fig. S14). The band pattern of collagen fibrils indicates that there were no crystals inside collagen fibrils. This is due to that the poly(acrylic aicd) absorbs calcium ions, reduces the concentration of calcium below the critical point of liquid-liquid phase separation and prohibits the confined mineralization process.Infiltration and transformation of ACC

The present study investigated the initiation and development of confined mineralization of ACC within collagen fibrils. The coexistence of crystalline phase and amorphous phase was observed on the surface and interior of fibrils during collagen mineralization (Fig. 3b), After 48 h of mineralization, distinct structures and morphologies were identified in different parts of a fibril in which there was distribution of spherical droplets around the collagen fibril (the upper box in Fig. 4a). The SAED pattern shows a diffuse characteristic band of ACC (Fig. 4b). In the other part of the same fibril (the lower box in Fig. 4a), there were nanoparticles instead of droplets. The SAED pattern confirmed the phase as vaterite (Fig. 4c). The ring-type diffraction pattern discloses a polycrystalline texture of vaterite, which provides direct evidence of the ACC phase transformation into vaterite. Although the vaterite phase was identified with SAED, it was not detectable with FTIR due to either the instability or insufficient amount of the material.

The above observations confirm the infiltration process of ACC into collagen fibrils and the phase transformation of ACC inside collagen fibrils. At the beginning of infiltration, spherical droplets attach on fibrils and change to thin film-like shape. Fluid characteristics of ACC facilitate the shape change of spherical droplets and facilitate the infiltration into the collagen fibril. Meanwhile, the amorphous-to-crystalline transition is energetically downhill.[38] The crystalline phase grows at the expense of the transient spherical ACC. ACC particles gradually shrink due to the expulsion of water during the crystallization process. The phase boundary between ACC and crystalline phase was evidently observed (Fig. 3b). This implies that the transformation of ACC into crystalline phase occurred through a secondary nucleation mechanism.[39,40] After 72 h, the transformation of ACC into crystalline phase was almost complete. The intermediate unstable vaterite phase had transformed into the most stable calcite via a dissolution-reprecipitation process.[41] During the secondary nucleation, existing nanoparticles could template the orientation of neighboring forming crystal.[40] Simultaneously, the collagen matrix played an important role in stress relaxation, which provided the sites for co-orientation of nanoparticles on the macroscopic scale.[31] This also explains the change of the ring-type diffraction pattern in intermediate course (Fig. 4c) to the final arc-shaped diffraction spots (Fig. 2c inset).

Driving force of ACC infiltration into collagen fibrils

The collagen fibrils mineralization of calcium carbonate has been achieved. We further investigated the nature of the driving force of ACC infiltrating into collagen fibrils. Capillary forces or electrostatic interaction can contribute to the ACC infiltration.[42,27] Previous studies showed that Mg^{2+} strongly influences the wetting behavior of ACC and straightforwardly controls mineralization sites in organic-inorganic hybrids.[34] To study the driving force of ACC penetrating into fibrils, Mg^{2+} was incorporated into the mineralization process as Mg^{2+}/Ca^{2+} in a ratio of 1/1. It was found that minerals with irregular morphology in the periphery of fibrils did not infiltrate into fibrils (Fig. 5).
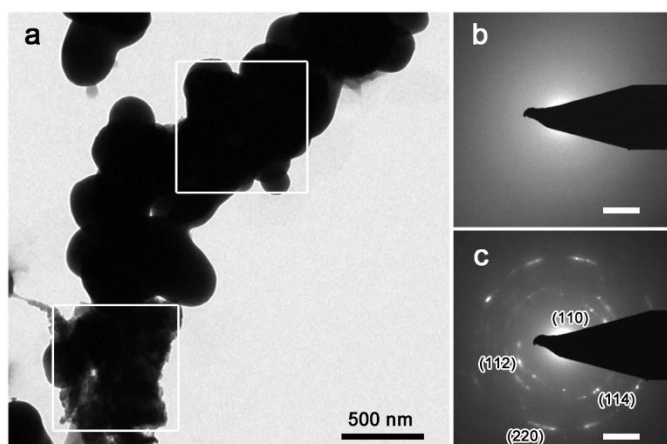

Fig. 4. Mineralization of reconstituted collagen fibrils after 48 h of mineralization. (a) TEM image of (b) isolated fibril and (c) SAED patterns of different parts of the fibril in (a).
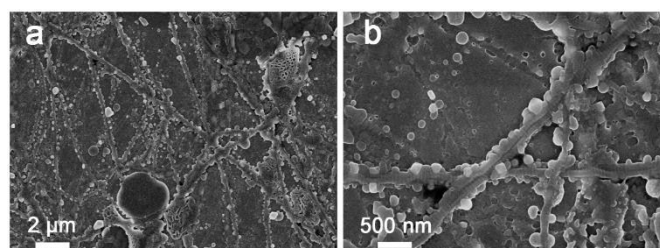

Fig. 5. SEM images of extrafibrillar mineralization in the presence of magnesium ions in mineralization solution. (a) Low and (b) high magnification SEM images.

The size distribution of ACC and Mg-ACC (ACC with Mg^{2+}) in 3 h of mineralization was analyzed by dynamic light scattering (DLS) data. The bimodal distribution of ACC (Fig. 6a) was revealed with a dominant peak at 50 nm corresponding to the primary particle and another peak ranging from 200 to 1,000 nm, implying the aggregate of primary particles, which was

This journal is © The Royal Society of Chemistry 2015

J. Mater. Chem. B, 2015, **00**, 1-3 | **5**

ARTICLE

Journal Name

consistent with TEM data (Fig. S5c). However, a narrow size distribution of Mg-ACC (Fig. 6c) was revealed with the apparent average diameter of 40 nm, which was smaller than ACC. The distribution of Mg-ACC was uniform in solution with almost no coalescence (Fig. S15). EDS analysis proved the existence of the magnesium element in the amorphous phase and the incorporation of Mg^{2+} into ACC (Fig. S16). Since the bond length of Mg-O in ACC is shorter than that Ca-O distances, Mg ions stabilize the disordered structure of ACC and prevent amorphous phase from aggregating and crystallizing.[34,43]
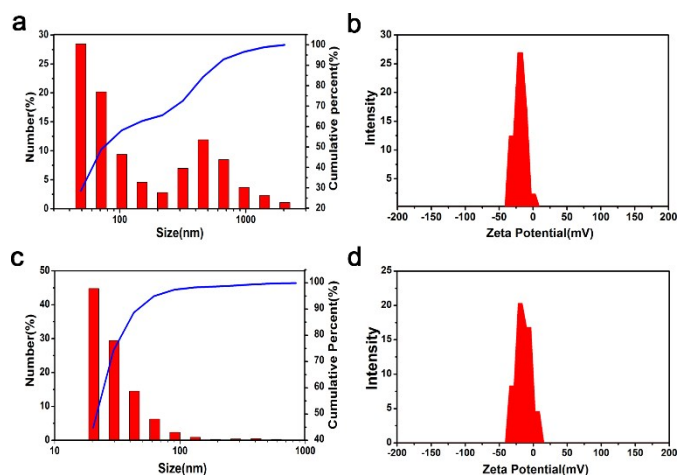

Fig. 6. Size distribution and surface charge of aggregated cluster species in solution. (a), (c) DLS and (b), (d) Zeta potential of droplets in mineralization solution in the absence and presence of magnesium ions, respectively.

The Zeta potential of ACC and Mg-ACC is -18.9 mV and -10.8 mV at pH 7.4, respectively (Fig. 6b and 6d). The negatively charged ACC is attracted to the positively charged gap regions of collagen fibrils through electrostatic interaction. It has been demonstrated that the negatively charged polymer-amorphous phase complex together with positively charged domains in collagen fibrils is essential for the mineral infiltration of bone apatite formation.[27] In the present study, there was no observation that the negatively charged Mg-ACC could be drawn into the fibrils, indicating that electrostatic interactions between amorphous phase and collagen fibrils is not the only dominant factor during collagen fibrils mineralization of calcium carbonate.[44] If amorphous phase just diffuses into collagen fibrils from the gap regions, the smaller sized Mg-ACC may be more liable to infiltrate. However, the present study observed that the large sized ACC rather than small sized Mg-ACC can infiltrate into collagen fibrils. This infers that capillary forces control the infiltration process of amorphous phase.[19,42] It is found that the crystallization of ACC can be prohibited by the addition of magnesium ions, which may also change the driving force to infiltrate into collagen fibrils. The uptake of liquid-like amorphous phase into collagen fibrils was ascribed to the gap region of collagen, which is analogous to water infiltration into pores as a result of capillary effects. The phase boundary between the amorphous phase and void space was essential to create the interface, which was acted upon by Laplace pressure

and drove amorphous phase into void space.[45] Additionally, the wettability of ACC was tuned by Mg^{2+}, meaning that the surface chemical composition of Mg-ACC was changed.[46] The wet behaviour had a profound effect on capillary forces, and it was likely that Mg-ACC only attaches to the collagen fibril rather than penetrates into the fibril.

Conclusions

In the present study, the confined mineralization of calcium carbonate within collagen fibrils has been achieved. The initiation and development of confined mineralization of ACC within collagen fibrils was intensively investigated, and the infiltration of ACC into collagen fibrils as well as the transformation of infiltrated ACC was disclosed. The nature of the driving force of ACC infiltrating into collagen fibrils was also examined. Briefly, the confined mineralization process of calcium carbonate within collagen fibrils is as follows. The negatively charged ACC droplets were attracted to positively charged gap region of collagen fibrils through electrostatic interaction. Due to highly hydrated and liquid-like characteristics, ACC can wet and coat the surface of collagen fibrils. This allows ACC to penetrate collagen fibrils with the aid of capillary force. Meanwhile, the transition of thermodynamics unstable amorphous phase into stable crystalline phase was energetically favorable through a secondary nucleation mechanism. Collagen matrix relaxed the stress of the transition of amorphous to crystalline, which facilitated the co-orientation of nanoparticles on the macroscopic scale. This investigation not only provides evidence of the confinement effects in biomineralization, but also facilitates the understanding of the bone formation process in vivo. The present study may also shed light on a promising strategy for bioprocess-inspired synthesis of advanced materials.

Acknowledgements

Notes and references

1   G. Mayer, *Science*, 2005, **310**, 1144-1147.
2   F. Bouville, E. Maire, S. Meille, B. Van de Moortele, A. J. Stevenson and S. Deville, *Nat. Mater.*, 2014, **13**, 508-514.
3   E. Munch, M. E. Launey, D. H. Alsem, E. Saiz, A. P. Tomsia and R. O. Ritchie, *Science*, 2008, **322**, 1516-1520.
4   X. G. Liu, K. L. Lin, C. T. Wu, Y. Y. Wang, Z. Y. Zou and J. Chang, *Small*, 2014, **10**, 152-159.

6 | *J. Mater. Chem. B*, 2015, **00**, 1-3

This journal is © The Royal Society of Chemistry 2015

5   H. Ping, H. Xie, B. L. Su, Y. B. Cheng, W. M. Wang, H. Wang, Y. C. Wang, J. Y. Zhang, F. Zhang and Z. Y. Fu, *J. Mater. Chem. B*, 2015, **3**, 4496-4502.

6   X. L. Wang, H. Xie, B. L. Su, Y. B. Cheng, J. J. Xie, H. Ping, M. H. Wang, J. Y. Zhang, F. Zhang and Z. Y. Fu, *J. Mater. Chem. B*, 2015, **3**, 5951-5956.

7   H. Zeng, J. J. Xie, H. Xie, B. L. Su, M. H. Wang, H. Ping, W. M. Wang, H. Wang and Z. Y. Fu, *J. Mater. Chem. A*, 2015, Doi: 10. 1039/C5TA04649A.

8   W. L. Noorduin, A. Grinthal, L. Mahadevan and J. Aizenberg, *Science*, 2013, **340**, 832-837.

9   F. Natalio, T. P. Corrales, M. Panthofer, D. Schollmeyer, I. Lieberwirth, W. E. Muller, M. Kappl, H. J. Butt and W. Tremel, *Science*, 2013, **339**, 1298-1302.

10 J. Mahamid, B. Aichmayer, E. Shimoni, R. Ziblat, C. H. Li, S. Siegel, O. Paris, P. Fratzl, S. Weiner and L. Addadi, *Proc. Natl. Acad. Sci. U. S. A.*, 2010, **107**, 6316-6321.

11 L. B. Gower, *Chem. Rev.*, 2008, **108**, 4551-4627.

12 Y. Levi-Kalisman, G. Falini, L. Addadi and S. Weiner, *J. Struct. Biol.*, 2001, **135**, 8-17.

13 Y. Politi, T. Arad, E. Klein, S. Weiner and L. Addadi, *Science*, 2004, **306**, 1161-1164.

14 J. Seto, Y. R. Ma, S. A. Davis, F. Meldrum, A. Gourrier, Y. Y. Kim, U. Schilde, M. Sztucki, M. Burghammer, S. Maltsev, C. Jager and H. Colfen, *Proc. Natl. Acad. Sci. U. S. A.*, 2012, **109**, 3699-3704.

15 J. A. Wesson and M. D. Ward, *Curr. Opin. Nephrol. Hy.*, 2006, **15**, 386-393.

16 M. Hildebrand, *Chem. Rev.*, 2008, **108**, 4855-4874.

17 M. Maas, P. Guo, M. Keeney, F. Yang, T. M. Hsu, G. G. Fuller, C. R. Martin and R. N. Zare, *Nano Lett.* 2011, **11**, 1383-1388.

18 B. Cantaert, E. Beniash and F. C. Meldrum, *Chem. Eur. J.*, 2013, **19**, 14918-14924.

19 C. J. Stephens, S. F. Ladden, F. C. Meldrum and H. K. Christenson, *Adv. Funct. Mater.*, 2010, **20**, 2108-2115.

20 Y. Y. Kim, N. B. J. Hetherington, E. H. Noel, R. Kroger, J. M. Charnock, H. K. Christenson and F. C. Meldrum, *Angew. Chem. Int. Ed.*, 2011, **50**, 12572-12577.

21 A. S. Schenk, E. J. Albarracin, Y. Y. Kim, J. Ihli and F. C. Meldrum, *Chem. Commun.*, 2014, **50**, 4729-4732.

22 A. K. Rajasekharan and M. Andersson, *Cryst. Growth Des.*, 2015, **15**, 2775-2780.

23 J. D. Currey, *Science*, 2005, **309**, 253-254.

24 G. E. Fantner, T. Hassenkam, J. H. Kindt, J. C. Weaver, H. Birkedal, L. Pechenik, J. A. Cutroni, G. A. G. Cidade, G. D. Stucky, D. E. Morse and P. K. Hansma, *Nat. Mater.*, 2005, **4**, 612-616.

25 A. George and A. Veis, *Chem. Rev.*, 2008, **108**, 4670-4693.

26 J. P. R. O. Orgel, T. C. Irving, A. Miller and T. J. Wess, *Proc. Natl. Acad. Sci. U. S. A.*, 2006, **103**, 9001-9005.

27 F. Nudelman, K. Pieterse, A. George, P. H. H. Bomans, H. Friedrich, L. J. Brylka, P. A. J. Hilbers, G. de With and N. A. J. M. Sommerdijk, *Nat. Mater.*, 2010, **9**, 1004-1009.

28 L. N. Niu, K. Jiao, Y. P. Qi, C. K. Y. Yiu, H. Ryou, D. D. Arola, J. H. Chen, L. Breschi, D. H. Pashley and F. R. Tay, *Angew. Chem. Int. Ed.*, 2011, **50**, 11688-11691.

29 B. Zhou, L. N. Niu, W. Shi, W. Zhang, D. D. Arola, L. Breschi, J. Mao, J. H. Chen, D. H. Pashley and F. R. Tay, *Adv. Funct. Mater.*, 2014, **24**, 1895-1903.

30 L. N. Niu, K. Jiao, H. Ryou, C. K. Y. Yiu, J. H. Chen, L. Breschi, D. D. Arola, D. H. Pashley and F. R. Tay, *Angew. Chem. Int. Ed.*, 2013, **52**, 5762-5766.

31 F. Nudelman, P. H. H. Bomans, A. George, G. de With and N. A. J. M. Sommerdijk, *Faraday Discuss.*, 2012, **159**, 357-370.

32 J. Ihli, W. C. Wong, E. H. Noel, Y. Y. Kim, A. N. Kulak, H. K. Christenson, M. J. Duer and F. C. Meldrum, *Nat. Commun.*, 2014, **5**, 3169-3178.

33 J. F. Ye, W. Liu, J. G. Cai, S. A. Chen, X. W. Zhao, H. H. Zhou and L. M. Qi, *J. Am. Chem. Soc.*, 2011, **133**, 933-940.

34 J. K. Berg, T. Jordan, Y. Binder, H. G. Borner and D. Gebauer, *J. Am. Chem. Soc.*, 2013, **135**, 12512-12515.

35 M. Faatz, F. Grohn and G. Wegner, *Adv. Mater.*, 2004, **16**, 996-1000.

36 B. Cantaert, Y. Y. Kim, H. Ludwig, F. Nudelman, N. A. J. M. Sommerdijk and F. C. Meldrum, *Adv. Funct. Mater.*, 2012, **22**, 907-915.

37 J. Baumgartner, A. Dey, P. H. H. Bomans, C. Le Coadou, P. Fratzl, N. A. J. M. Sommerdijk and D. Faivre, *Nat. Mater.*, 2013, **12**, 310-314.

38 Y. U. T. Gong, C. E. Killian, I. C. Olson, N. P. Appathurai, A. L. Amasino, M. C. Martin, L. J. Holt, F. H. Wilt and P. U. P. A. Gilbert, *Proc. Natl. Acad. Sci. U. S. A.*, 2012, **109**, 6088-6093.

39 Y. Politi, R. A. Metzler, M. Abrecht, B. Gilbert, F. H. Wilt, I. Sagi, L. Addadi, S. Weiner and P. U. P. A. Gilbert, *Proc. Natl. Acad. Sci. U. S. A.*, 2008, **105**, 17362-17366.

40 C. E. Killian, R. A. Metzler, Y. U. T. Gong, I. C. Olson, J. Aizenberg, Y. Politi, F. H. Wilt, A. Scholl, A. Young, A. Doran, M. Kunz, N. Tamura, S. N. Coppersmith and P. U. P. A. Gilbert, *J. Am. Chem. Soc.*, 2009, **131**, 18404-18409.

41 M. H. Nielsen, S. Aloni and J. J. De Yoreo, *Science*, 2014, **345**, 1158-1162.

42 M. J. Olszta, X. G. Cheng, S. S. Jee, R. Kumar, Y. Y. Kim, M. J. Kaufman, E. P. Douglas and L. B. Gower, *Mater. Sci. Eng. R*, 2007, **58**, 77-116.

43 Y. Politi, D. R. Batchelor, P. Zaslansky, B. F. Chmelka, J. C. Weaver, I. Sagi, S. Weiner and L. Addadi, *Chem. Mater.*, 2010, **22**, 161-166.

44 B. Cantaert, E. Beniash and F. C. Meldrum, *J. Mater. Chem. B*, 2013, **1**, 6586-6595.

45 Q. B. Wang, B. Su, H. Liu and L. Jiang, *Adv. Mater.*, 2014, **26**, 4889-4894.

46 Y. Tian and L. Jiang, *Nat. Mater.*, 2013, **12**, 291-292.

Table of contents entry
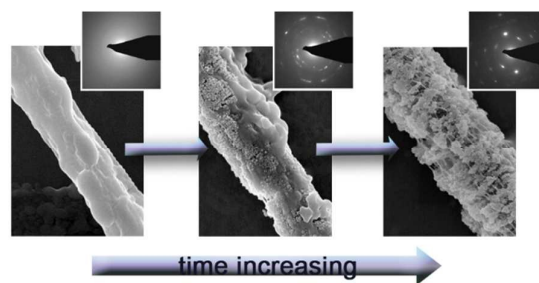
The amorphous calcium carbonate infiltrates into collagen fibrils and transforms into co-oriented crystalline phase under the function of confinement.